Marine Chemistry 267 (2024) 104454

Contents lists available at ScienceDirect

Marine Chemistry

journal homepage: www.elsevier.com/locate/marchem

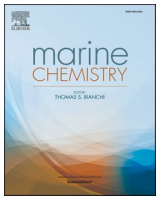

Two-dimensional determination of dissolved manganese in sediment porewaters

Aurélia Mouret [a,*], Constance Choquel [a,b], Aubin Thibault de Chanvalon [c], Florian Cesbron [d], Thierry Jauffrais [a,e], Didier Jézéquel [f,g], Patrick Launeau [a], Anthony Barbe [a], Romain Levrard [a], Alan Nicol [a,h], Céline Charbonnier [i], Edouard Metzger [a]

[a] Univ Angers, Nantes Université, Le Mans Université, CNRS, Laboratoire de Planétologie et Géosciences, LPG UMR 6112, 49000 Angers, France
[b] Aix Marseille Université, Univ. de Toulon, CNRS, IRD, MIO, 13288 Marseille, France
[c] Université de Pau et des Pays de l'Adour, E2S UPPA, CNRS, IPREM, Pau, France
[d] LUSAC - Laboratoire Universitaire des Sciences Appliquées de Cherbourg, 60 rue Max-Pol Fouchet, CS 20082, 50130 Cherbourg-en-Cotentin, France
[e] Ifremer, IRD, Univ Nouvelle-Calédonie, Univ La Réunion, CNRS, UMR 9220 ENTROPIE, RBE/LEAD, 101 Promenade Roger Laroque, 98897 Noumea, New Caledonia
[f] Université Paris Cité, Institut de Physique du Globe de Paris, CNRS, 75005 Paris, France
[g] INRAE & Université Savoie Mont Blanc, UMR CARRTEL, 74200 Thonon-les-Bains, France
[h] Department of Clinical Neuroscience, Division of Eye and Vision, St. Erik Eye Hospital, Karolinska Institute, Stockholm, Sweden
[i] Université de Bordeaux, CNRS, UMR 5805 Environnements Paléoenvironnements Océaniques et Continentaux (EPOC), Pessac, 33615, France

ARTICLE INFO

Keywords:
High-resolution
2D-DET
Sediment microenvironments
Bioirrigation

ABSTRACT

We present a new method for imaging dissolved manganese at millimeter scale by coupling DET (diffusive equilibrium in thin film) and colorimetric techniques. The method is an adaptation of the porphyrin approach for the measurement of dissolved Mn by substitution of Mn(II) and Mn(III) to Cd in the Cd(II)–POR complex. Optimization of the Cd-POR concentrations was required for transposition to 2D-DET. A commercial flatbed scanner and a hyperspectral camera were used for imaging. Using the hyperspectral camera, detection limit is about 5 μM and measuring range is up to 520 μM. The method was applied on the field in a tidal mudflat of the French Atlantic coast and in sediments inhabited by polychaetes. These first images allowed to precisely describe two-dimensional millimeter features such as burrows and highlighted the role of bioirrigation in benthic Mn fluxes. This new technique offers the possibility to investigate the reactivity of microenvironments towards dissolved Mn in two dimensions in a wide range of laboratory and *in situ* studies using a non-destructive tool.

1. Introduction

Manganese is a major redox element in marine environments. In sediments, manganese is known to cycle through burial of oxidized manganese below the redox boundary, reductive dissolution of oxidized manganese to dissolved Mn(II), upward diffusion of dissolved Mn(II), and reoxidation of Mn(II) to insoluble Mn(IV) above the redox boundary. In addition, Mn(III) has been documented as a frequent intermediate in Mn redox transformations in both the solid (or adsorbed) phase (Anschutz et al., 2005; Murray et al., 1985) and the dissolved phase (Madison et al., 2013; Oldham et al., 2017c; Thibault de Chanvalon and Luther, 2019; Trouwborst et al., 2006). Mn reduction is coupled to organic matter mineralization processes because Mn oxides can be used as terminal electron acceptors in anaerobic environments (Canfield et al., 1993a; Froelich et al., 1979), and thus Mn plays an important role in many biogeochemical cycles (carbon, nitrogen, sulfur, oxygen, iron) (Lewis and Landing, 1991; Tebo, 1991; Burdige, 1993; Thamdrup et al., 1994; Gobeil et al., 1997; Luther et al., 1997; Luther, 2010; Oldham et al., 2017a, 2017b; Owings et al., 2021). Establishing the distribution of dissolved manganese is essential for understanding redox processes in sedimentary deposits.

Sediment cores can be sampled and then pressed or sliced and centrifuged, or rhizons can be inserted to provide access to porewaters and allow measurements of dissolved Mn using colorimetric techniques (Burle and Kirby-Smith, 1979; Chiswell et al., 1990; Madison et al., 2011; Soto-Neira et al., 2011a), AAS (Atomic Absorption Spectrometry), ICP-MS (Inductively Coupled Plasma-Mass Spectroscopy) or ICP-OES (Inductively Coupled Plasma-Optical Emission Spectroscopy).

* Corresponding author.
E-mail address: aurelia.mouret@univ-angers.fr (A. Mouret).

https://doi.org/10.1016/j.marchem.2024.104454
Received 13 March 2024; Received in revised form 22 August 2024; Accepted 13 September 2024
Available online 14 September 2024

However, these types of sampling methods limit the vertical spatial resolution of the data due to the thickness of the sediment slices (or the squeezer device used) and provide only access to a one-dimensional view of sediments. The other problem with sediment slicing followed by squeezing or centrifugation is that the observed chemical profiles represent the net result of chemical reactions that occur when spatially separated chemical species are mixed during the porewater extraction process. This can be a significant problem in organic-rich sediments where geochemical gradients occur on spatial scales of less than a millimeter. The development of high spatial resolution techniques such as voltammetric microelectrodes, DET (diffusive equilibrium in thin film) and DGT (diffusive gradient in thin films) has improved the characterization of sharp gradients (Brendel and Luther, 1995; Davison et al., 1994; Dočekalová et al., 2002; Shuttleworth et al., 1999; Zhang et al., 1995) and stimulated ideas about the role of microniches in sediments. The role of macrofauna on three-dimensional heterogeneity in sediments has been studied, including heterogeneous and authigenic formation of manganese oxyhydroxides in or around biogenic structures like burrows (*e.g.* Aller et al., 1990; Swinbanks and Shirayama, 1984). Numerous studies have demonstrated that bioturbation and bioirrigation with passive or active flushing of burrows strongly impact Mn cycle (Aller et al., 1990; Canfield et al., 1993b; Sundby and Silverberg, 1985; Thamdrup et al., 1994). However, direct mapping observations of three-dimensional structures in porewater Mn distribution are scarce (Shuttleworth et al., 1999) and require the improvement of adapted methods.

In the last years, numerous developments have been realized in methods for high spatial resolution imaging of solutes related to organic matter mineralization and redox reactions by coupling DET and colorimetric methods (Jézéquel et al., 2007; Robertson et al., 2008; Pagès et al., 2011; Cesbron et al., 2014; Bennett et al., 2015; Metzger et al., 2016; Le Houedec et al., 2019; Metzger et al., 2019; Kankanamge et al., 2020; Castillejos Sepúlveda et al., 2023). Here we present the development of a new colorimetric DET method for measuring 2D distributions of dissolved Mn concentrations in sediment porewaters. This new method is based on the protocol proposed by Madison et al. (2011) using α, β, γ, δ-tetrakis(4-carboxyphenyl)porphyrin (hereafter referred to as POR), whose kinetic approach allows the separate quantification of dissolved Mn(II) and Mn(III). Low-cost imaging was performed using a commercial flatbed scanner, while the hyperspectral camera was used to test possible improvements in detection sensitivity. Finally, a comparison with a more conventional analytical method for porewaters was carried out in sediments from an intertidal mudflat.

2. Material and methods

2.1. Principle of the colorimetric method

The principle is based on the substitution of Cd by Mn(II) and Mn(III) in the Cd(II)–POR complex due to the higher stability of the Mn–POR complex at pH of 7.5–8. The addition of imidazole catalyzes this substitution. For Mn(II), the substitution is complete in approximately 1 min (Ishii et al., 1982; Madison et al., 2011) and the Mn(II) of the Mn(II)–POR complex is immediately oxidized by dissolved oxygen to form Mn(III)–POR. As Mn(III) in natural water is stabilized by complexation with organic ligands, Mn(III) substitution is slower. The formation of Mn(III)–POR occurs *via* ligand exchange and the rate of Mn(III)–POR formation from Mn(III) is slower than that from Mn(II). Madison et al. (2011) showed that the rate of POR complexation of soluble Mn(III) depends on the strength of the original Mn(III) complex. The stronger the initial Mn(III) complex, the slower the rate of POR complexation. They showed that complexation of 95 % of Mn(III) occurs within approximately 5–15 min for Mn(III)-pyrophosphate, whereas more than 24 h are required for Mn(III)- Desferioxamine-B, which is a strong ligand. The dye formed by the substitution of Cd by Mn is yellowish. Ishii et al. (1982) showed that the strong absorption band (the Soret band) for POR is at 415 nm, for Cd(II)–POR complex at 433 nm and for Mn(III)–POR at 468–470 nm (extinction coefficient ε468 = 95,500 M^{-1} cm^{-1} (Thibault de Chanvalon and Luther, 2019; Madison et al., 2011)). Several weaker absorption bands are also present, located at 500–650 nm (the Q band) (Soto-Neira et al., 2011a).

2.2. DET gels

2.2.1. DET gel preparation

The 1 mm or 0.5 mm-thick polyacrylamide DET gels were prepared according to Jézéquel et al. (2007), adapted from Davison and Zhang (1994). Solutions of acrylamide (30 %, Roth, CAS number 79–06-1), bisacrylamide (2 %, Roth, CAS number 110–26-9), TEMED (Roth, CAS number 110–18-9) and ammonium persulfate (APS; 1 %, Sigma-Aldrich, CAS number 7727-54-0) were rapidly mixed and cast between two plates separated by a spacer. Polymerization occurred after 15 min at room temperature. The gel was rinsed and stored in deionized water (Millipore Milli-Q® system) until use. Before hydration, thickness of the gels was 0.8 mm or 0.4 mm but reached about 1 mm or 0.5 mm, respectively, after 1 h hydration.

2.2.2. Gel probe

The probe was a 1 mm or 0.5 mm thick polyacrylamide DET gel. The gel was mounted on a polycarbonate plate and covered with a PVDF hydrophilic membrane (0.2 µm, Durapore®), which was attached to the plate with PVC adhesive tape. In order to prevent an oxidation of Mn(II) present in the anoxic sediment during gel probe deployment, the probe was deoxygenated by bubbling nitrogen in deionized water (Millipore Milli-Q® system) at least 5 h before deployment. Probes were deployed into sediment for 5 h to allow porewater solutes to diffuse into the gel and reach concentration equilibrium.

2.2.3. Standard gel

The standard gel was a polyacrylamide DET gel with a thickness of 1 mm or 0.5 mm (according to the thickness of the gel probe). For calibration, the gel was set between two pieces of polycarbonate plate, tightened together with eight small clamps, one of which was designed to have seven wells (schematic of the device detailed in Cesbron et al. (2014), supporting information). These wells were filled with 3.5 mL of standard solutions, covered with caps and left for 1 h for diffusive equilibration. Mn standard solutions were prepared from $MnCl_2$, $4H_2O$ salt (Sigma, CAS number 13446–34-9). All Mn standards were prepared in a solution of appropriate ionic strength just prior to calibration. To study Fe interference, Fe standard solutions were prepared from Mohr's salt ($(NH_4)_2Fe(SO_4)_2$, $6H_2O$, Prolabo Normapur, CAS number 7783-85-9). Due to the rapid oxidation of Fe^{2+}, Fe standards were prepared with a deoxygenated solution and then equilibrated with the standard gel in a glove bag under nitrogen atmosphere.

2.2.4. Reagent gel

Reagent gel was 1 mm-thick polyacrylamide hydrogel. Gels were equilibrated for 30 min with 50 mL of reagent solution in a plastic box covered with aluminum foil because of the light sensitivity of the reagent. The coloring reagent solution was prepared in several steps. First, a 0.48 mM porphyrin solution (1) was prepared by dissolving some α, β, γ, δ-tetrakis(4-carboxyphenyl)porphyrin powder (Sigma-Aldrich, CAS number 14609–54-2) in a 0.1 M NaOH solution. Because POR is photosensitive, this solution was stored in a polypropylene bottle wrapped in aluminum foil. Secondly, a solution of 0.013 M sodium tetraborate (Sigma-Aldrich, CAS number 1330-43-4), 0.16 M imidazole (Acros Organic, CAS number 288–32-4) and 0.021 M HCl (2) was prepared and pH was adjusted to 8.0 by adding small amounts of 3 M HCl. A 2.9 mM $CdCl_2$ solution (3) was prepared by dissolving $CdCl_2$ salt (Fluka, CAS number 10108–64-2) in Milli-Q® water. This last chemical is considered hazardous due to its acute toxicity and must therefore be handled with all necessary precautions. Finally, just before equilibration

with the reagent gel, the three solutions were mixed in the proportions 2/3 (1) + 2/9 (2) + 1/9 (3) to finalize the reagent solution.

2.2.5. Gel assemblage for colorimetric reaction

After equilibration, reagent gel was removed from the box, quickly drained and laid on a white plate. After wiping away any residual drops of reactive solution, the probe gel (*i.e.* the one deployed in the field) or the standard gel was laid onto the reagent gel. The gel assemblage was then covered by a clean cellulose acetate film to prevent evaporation and quickly placed in a non-transparent box away from the light (due to the photosensitivity of the reagent). After 35 min of reaction at room temperature (~20 °C), the gel assemblage was scanned to acquire the 2D manganese distribution.

2.3. Imagery

2.3.1. Imagery from commercial flatbed scanner

A simple commercial flatbed scanner (Canon Canoscan LiDE 152600F) was used to obtain an image of the assembled gels. From scanned images, intensity of the 2D probe coloration was processed using ImageJ® software (Schneider et al., 2012). Images were first cropped (5 mm) to avoid edge effects and then decomposed into primary color intensities (red, green and blue at a wavelength resolution of approximately 140 nm), each of which was converted to a grey-scale image. The blue color intensity was found to give the most sensitive response as the dye formed is yellowish. A region of interest (ROI) corresponding to a circle of approximately 15 mm diameter (*i.e.* 30,000 pixels at the chosen resolution) was selected for each zone of the "standard gel"; each circle was a zone of equilibration of the gel with a standard solution.

2.3.2. Hyperspectral data acquisition and treatment for Mn mapping

In order to quantify dissolved Mn concentrations with high sensitivity, images of the two superimposed gels were acquired after completion of the colorimetric reaction using a 160-channel HySpex VNIR 1600 hyperspectral camera. The camera was set up to scan samples with a spectral resolution of 4.5 nm and a sampling step of 3.7 nm, covering a spectral range of 400 to 900 nm and a spatial resolution of 60 × 60 μm per pixel. However, the quantification of dissolved Mn concentration based on this imaging technique was not direct and required the following image processing, performed here using the ENVI classic software: (1) The hyperspectral camera obtained reflectance spectra. The reflectance was calculated by dividing each column of the analyzed image by the mean intensity of the light reflected by the white reference panel Spectralon (~99 % reflectance in the 400–900 nm range) scanned alongside, in order to avoid the residual non-uniformity of the sensor. (2) In order to obtain the most accurate image as possible, it was necessary to remove the background noise corresponding to erratic pixels (for example, due to dust or air bubbles). This is a statistical treatment ("minimum noise fraction" function) retaining only the informative pixels. (3) This step was dedicated to the calculation of the transmittance spectrum. From these spectra, Mn concentration could be calculated. An optical model used by Launeau et al. (2018) and Le Houedec et al. (2019) was applied to our gel images to calculate the transmittance signals from the measured reflectance signals. The spectral intensities were adjusted in the 850–920 nm spectral window, where the transmittance signal is not affected by chemical reactions. Therefore, a transfer function was used for converting the transmittance signal obtained from the analysis of the calibration gel at 470 nm into concentration for a concentration range between 0 and 100 μM and at 500 nm for concentrations between 100 and 500 μM.

2.4. Method optimization for gel technique and interference tests

An adaptation of the reagent was necessary because the ratio reagent gel thickness /probe or standard gel thickness (ratio of 2 or 1, depending on the gel thickness) is not comparable to the ratio reagent volume/sample volume used in Madison et al. (2011) (ratio of 30). To increase the measuring range and counteract the effect of chloride ions in seawater, which can form cadmium chloride complexes and destroy the Cd-POR complex (Thibault de Chanvalon and Luther, 2019), the reagent has been optimized by increasing the Cd-POR concentration. The method was also optimized by using thinner probe/standard gels to increase the reagent/probe or sample ratio (ratio of 2). Finally, due to the frequent coexistence of iron and manganese in porewaters over a wide range of ratios, the interference of dissolved iron was tested.

2.5. Validation with sediment

2.5.1. Field sampling

This technique was applied in an intertidal mudflat of the Bourgneuf Bay, located south of the Loire estuary on the French Atlantic coast. The bay is characterized by the presence of wild oyster reefs (Echappé et al., 2018) and oyster and mussel farming areas. Field sampling was conducted at low tide in March 2016 at an observation site named La Coupelasse (47°00′56.9"N 2°02′27.6"W), where sediment geochemistry was documented monthly by sampling three 10 cm diameter cores at each vertex of a 10 m equilateral triangle (cores A, B and C) (Metzger et al., 2019). Salinity was 29 and sediment temperature was 8 °C. 2D-DET probe was deployed within the sediment near core C for three hours for equilibration between gel and porewaters. The probe was then carefully collected with the surrounding sediment, representing a 3 cm thick slab, using a "jaw device"(Thibault de Chanvalon et al., 2015) and transported to the laboratory to achieve a total equilibration time of 5 h. The jaw device was then opened and the 2D-DET probe was immediately processed. Sediment cores were kept at *in situ* temperature until processing the following day.

2.5.2. Core processing and porewater analyses

Cores were sliced under nitrogen atmosphere every 2 mm to a depth of 2 cm, then every 5 mm to a depth of 5 cm, and finally every centimeter to a depth of 11 cm. Sediment slices were immediately centrifuged at 3500 rpm for 15 min and the supernatant was filtered through a 0.2 mm filter (RC25, Sartorius©) and acidified. Dissolved Mn analysis was performed after a 50-fold dilution with 1 % ultrapure nitric acid using an ICP-OES ICAP 6300 Thermo-Fischer.

2.5.3. Laboratory experiment with bioturbation

Sediment was collected during the same sampling event at La Coupelasse in March 2016 and taken back to the laboratory. The sediment was sieved through 0.5 mm mesh to remove macrofauna. After homogenization, the sediment was covered with constantly aerated natural seawater and left to equilibrate at room temperature for 7 weeks. 25 *Hediste diversicolor* were then added to the sediment to obtain a density of 250 ind/m^2. Gel deployment was carried out 10 days later to allow organisms to bioturbate the sediment. Mn and Fe gels were mounted on either side of the same probe, giving stackable Mn and Fe images. The Mn and Fe data were therefore superimposable. Fe reagent gel was prepared as described in Cesbron et al. (2014) and consisted of a 1-mm thick polyacrylamide gel. The colorimetric reagent for dissolved iron was ferrozine and ascorbic acid. The Fe image was acquired with a flatbed scanner and calibrated with Fe standards using the green channel, as described in Jézéquel et al. (2007).

3. Results and discussion

3.1. Method optimization

Some optimizations were necessary to adapt the spectrophotometric method to the gel technique and especially for analysis with a seawater matrix. There is a known interference from chlorine, which forms chloro-complexes with cadmium, breaking the Cd-POR complex and

inhibiting the reaction rate (Ishii et al., 1982; Thibault de Chanvalon and Luther, 2019). In the spectrophotometric method of Madison et al. (2011), samples were diluted to be within the range of 1–10 μM of dissolved Mn, which is the optimized concentration range for measurement, and to reduce chloride interference. Thibault de Chanvalon and Luther (2019) modified the method for low-level determination of dissolved Mn speciation in seawater by increasing the cadmium concentration in the reagent to limit dilution and chlorine interference. In our case, the protocol combining the gel layers resulted in a dilution factor of 2, using probe and reagent gels of the same thickness (1 mm). To increase the dilution factor, a thinner probe gel was used, inducing a 3-fold dilution when combining probe (0.5 mm) and reagent (1 mm) gels. The concentration of Cd-POR was doubled compared to the concentration defined in Madison et al. (2011) without reducing the sensitivity (Fig. 1 A, similar calibration slopes). These optimizations provide sufficient Cd-POR, even with chlorine interference, to measure relatively high concentrations of dissolved Mn (~300 μM) in seawater matrix (Fig. 1B).

3.2. Reaction kinetics, relaxation effect and spatial fidelity of the data

The DET gel exhibits a loss of spatial fidelity during deployment in the sediment, especially for sharp solute concentrations, because of lateral diffusion into the gel layer (Harper et al., 1997). After removal of the probe from the sediment, molecular diffusion within the gel induces relaxation of the signal, affecting concentration fidelity. Therefore, the time required to process the gel after retrieval, including the time required to complete the chemical reaction, should be as short as possible to limit alteration of the concentration gradients. Kinetics were established by scanning the assemblage of a standard gel and a reagent gel every 5 min and then every 10 min to measure the increase in intensity in the blue channel at the middle of the wells (Fig. 2A and B). No significant change was observed after 35 min. This time allows for the complete substitution of Cd by Mn(II) in the Cd-POR complex, and perhaps also ligand exchange for some weak Mn(III) complexes of a size that allows their diffusion in polyacrylamide gels. Dissolved Mn, which is the most labile, is therefore, quantified.

Figure 2C shows the evolution of a coloration profile across the edge of the 277 μM Mn standard-well as a function of time. The asymptotic diffusive profile centered at the well edge indicates that during the equilibration time between the standard solutions and the standard gel, dissolved Mn diffused laterally across the well edges. However, after contact with the reagent gel, the good superposition of the profiles indicates that the lateral diffusion of the yellowish dye is very limited. Consequently, the relaxation effect minimally affects the Mn distribution after the substitution of Mn for Cd in the Cd(II)–POR complex, as previously observed for nitrite, ammonium, iron and phosphorus (Cesbron et al., 2014; Metzger et al., 2016, 2019). Relaxation of the signal is therefore mostly controlled by the gel handling time (retrieval of gel probe from the sediment and handling of the reagent gel), which limits the spatial resolution at which data are reliable. For similar methods coupling DET and colorimetry, Metzger et al. (2016) showed that the location of a given solute production/consumption hotspot is precisely defined in two dimensions at submillimeter resolution (pixel resolution), but concentration fidelity is achieved at millimeter resolution due to relaxation effects.

3.3. Reproducibility of standardization

Several standard calibration curves were generated using the optimized protocol to assess the reproducibility of the method. The slopes and intercepts of the different standard calibration curves showed variations of 32 % and 14 %, respectively ($n = 13$) (Table 1). According to Charbonnier and Anschutz (2019), all the solutions that constitute the reagent can be stored in refrigerator for several months. However, the final reagent solution is unstable and must be prepared on the same day as Mn measurement. An evolution of the reagent over a few days was observed when already prepared solutions were used and mixed to obtain the final reagent with a higher reflectance value in the blue channel for the blank (Fig. 3). Nevertheless, no loss of sensitivity was observed. To bypass difficulties induced by variations in the final reagent, it is recommended to prepare a batch of reagents in sufficient quantity to be used for standard and probe gels for the same analysis session.

3.4. Fe interference assessment

Some authors reported interference with other metals (Ishii et al., 1982; Soto-Neira et al., 2011b). Other metal-POR complexes have Soret band absorbances at certain wavelengths close to the Soret band of Mn-POR. With the flatbed scanner, the images obtained are composed of primary color intensities (red, green and blue) with a wavelength

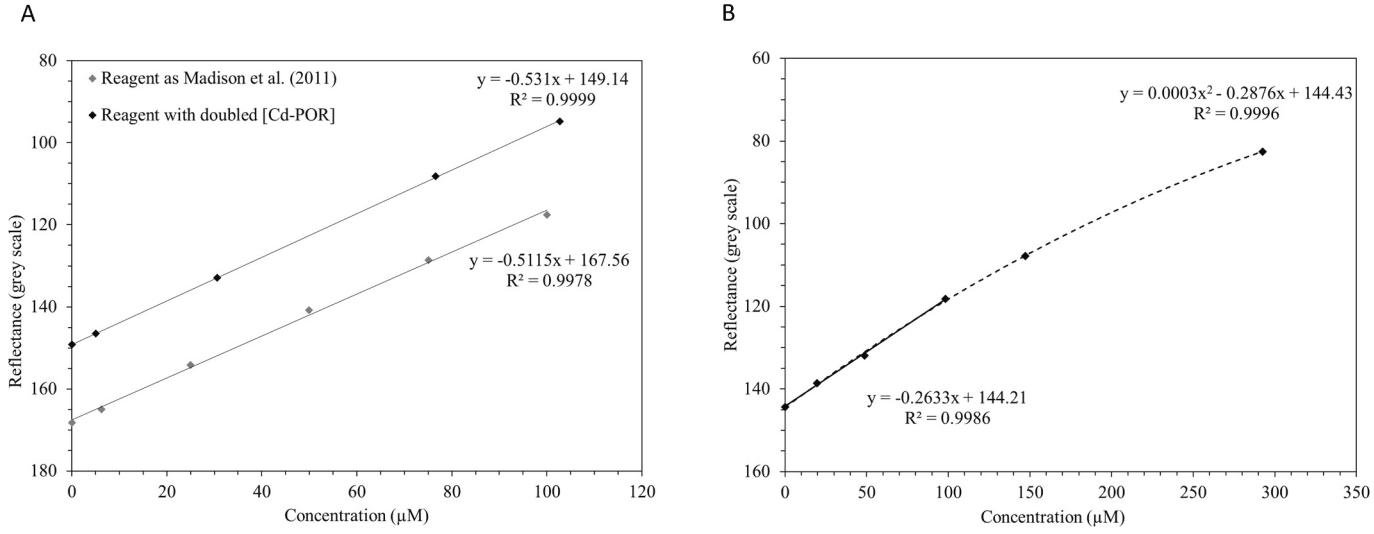

Fig. 1. A) Comparison of two calibration curves obtained using a flatbed scanner with different concentrations of Cd-POR in the reagent solution. Grey diamonds correspond to the reagent prepared according to Madison et al. (2011) and black diamonds correspond to the reagent with twice the concentration of Cd-POR. B). Linear calibration curve for Mn standards up to 100 μM and polynomial calibration curve for concentrations up to 300 μM, obtained after optimizing the gel technique with a seawater matrix.

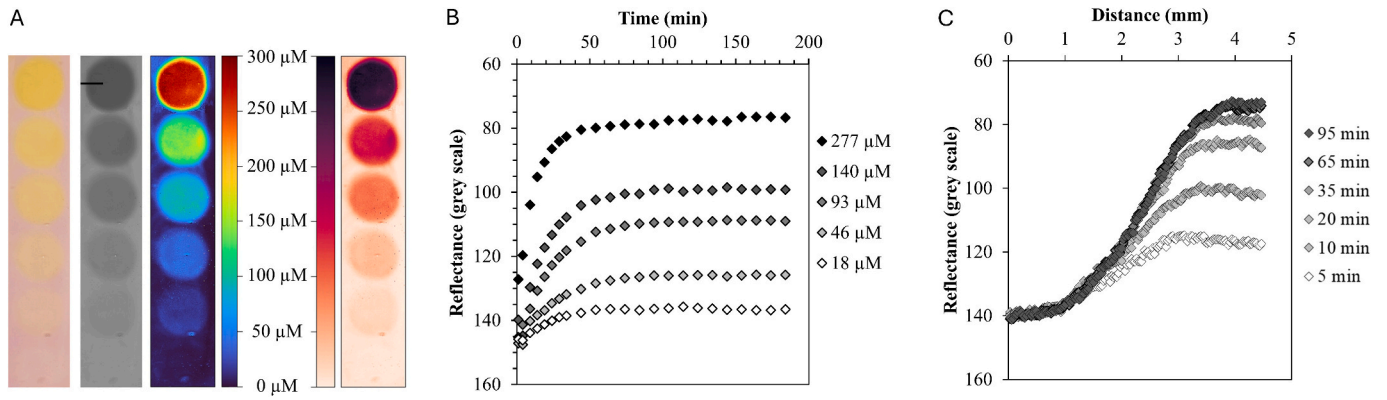

Fig. 2. Reaction kinetics established by scanning the assemblage of a standard gel and a reagent gel every 5 min and then every 10 min. (A) Images of the assembled gels with Mn concentrations ranging from 0 to 277 µM from bottom to top (0; 18; 46; 93; 140; 277 µM): on the left, image acquired with a flatbed scanner after 35 min; in the middle, blue channel image; on the right, images of the concentrations in false colors with a perceptually uniform rainbow color scale (Turbo) and a second uniform linear scale (Rocket) to improve image readability for all readers (B) Reflectance evolution of the standard curve over time. (C) Evolution of the profile over time across the well edge of the 277 µM standard (black line on the blue channel image A). (For interpretation of the references to color in this figure legend, the reader is referred to the web version of this article.)

Table 1
Calibration slopes, intercepts and R^2 of various standard calibration curves using freshly prepared and aged reagent solutions for final reagent mixing.

Reagent age	Calibration slope	Calibration intercept	R^2
1 h	−0.403	141.697	1.000
1 h	−0.401	133.559	0.980
1 h	−0.279	130.022	0.992
1 h	−0.735	98.450	0.987
1 h	−0.250	144.206	0.999
1 h	−0.335	114.358	0.981
1 h	−0.309	109.572	0.989
1 h	−0.364	137.345	0.991
7 d	−0.232	113.103	0.999
15 d	−0.406	88.989	0.976
1 h	−0.370	124.010	0.945
4 d	−0.392	110.556	0.985
5 d	−0.469	111.320	0.992

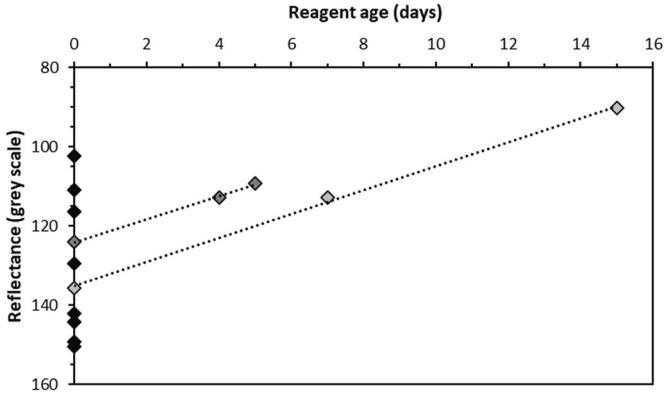

Fig. 3. Reflectance in the blue channel for the blanks of several standard calibration curves. The light and dark grey diamonds on the graph represent the time evolution of the blanks obtained with solutions already prepared for the final mixing of the reagent. The black diamonds correspond to the blanks obtained with freshly prepared reagent solutions. (For interpretation of the references to color in this figure legend, the reader is referred to the web version of this article.)

resolution of about 140 nm. Other metal-POR complexes can affect the reflectance measured in the blue channel. Iron interference was specifically assessed because of its high concentrations in coastal sediment porewaters. A very limited contribution of Fe was measured with a standard curve slope representing 3 % of the Mn slope, allowing to conclude that it is not a major interference (Fig. 4).

3.5. Measuring range and limit of detection

The protocol presented here using a flatbed scanner shows a linear relationship between manganese concentration and grey intensity for the blue channel within the range 0–100 µM. A second-degree polynomial relationship can be used for calibration up to 300 µM (**Fig. 1**B). The detection limit, calculated as 3-fold standard error of the blank, is 15.4 µM. Using the hyperspectral camera, manganese concentration and transmittance values at 470 nm (Mn Soret band) also present a linear relationship within the range 0–75 µM with a detection limit of 5.2 µM (Fig. 5). A polynomial relationship can also be applied up to 100 µM with a higher R-squared ($R^2 = 0.9871$ and $R^2 = 0.9997$ for the linear and polynomial relationships respectively). Cesbron et al. (2014) and Metzger et al. (2016) previously showed that the use of a hyperspectral camera provides better sensitivity and higher spectral resolution. The use of the Soret band wavelength of Mn (470 nm) improved the sensitivity of the measurement and also allowed to avoid interferences from other metals such as Fe (415 nm) (Soto-Neira et al., 2011a). For concentrations up to 520 µM, the 500 nm wavelength, located in the Q-band, a weaker absorption band of the POR complex, presents a lower

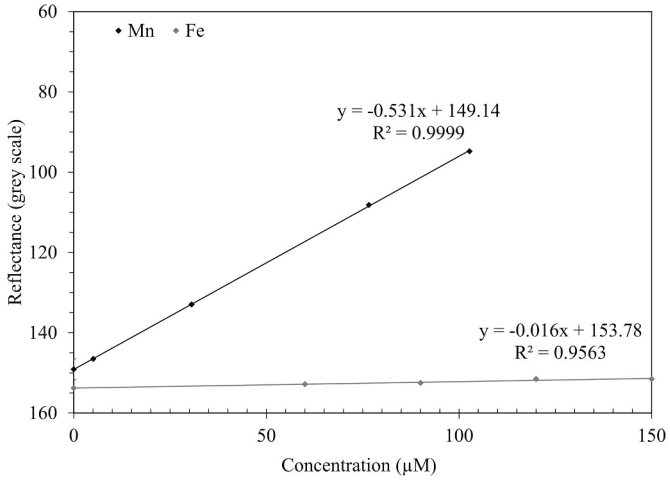

Fig. 4. Comparison of Mn standard calibration curve with Fe standard calibration curve to assess the potential interference of Fe-POR complex.

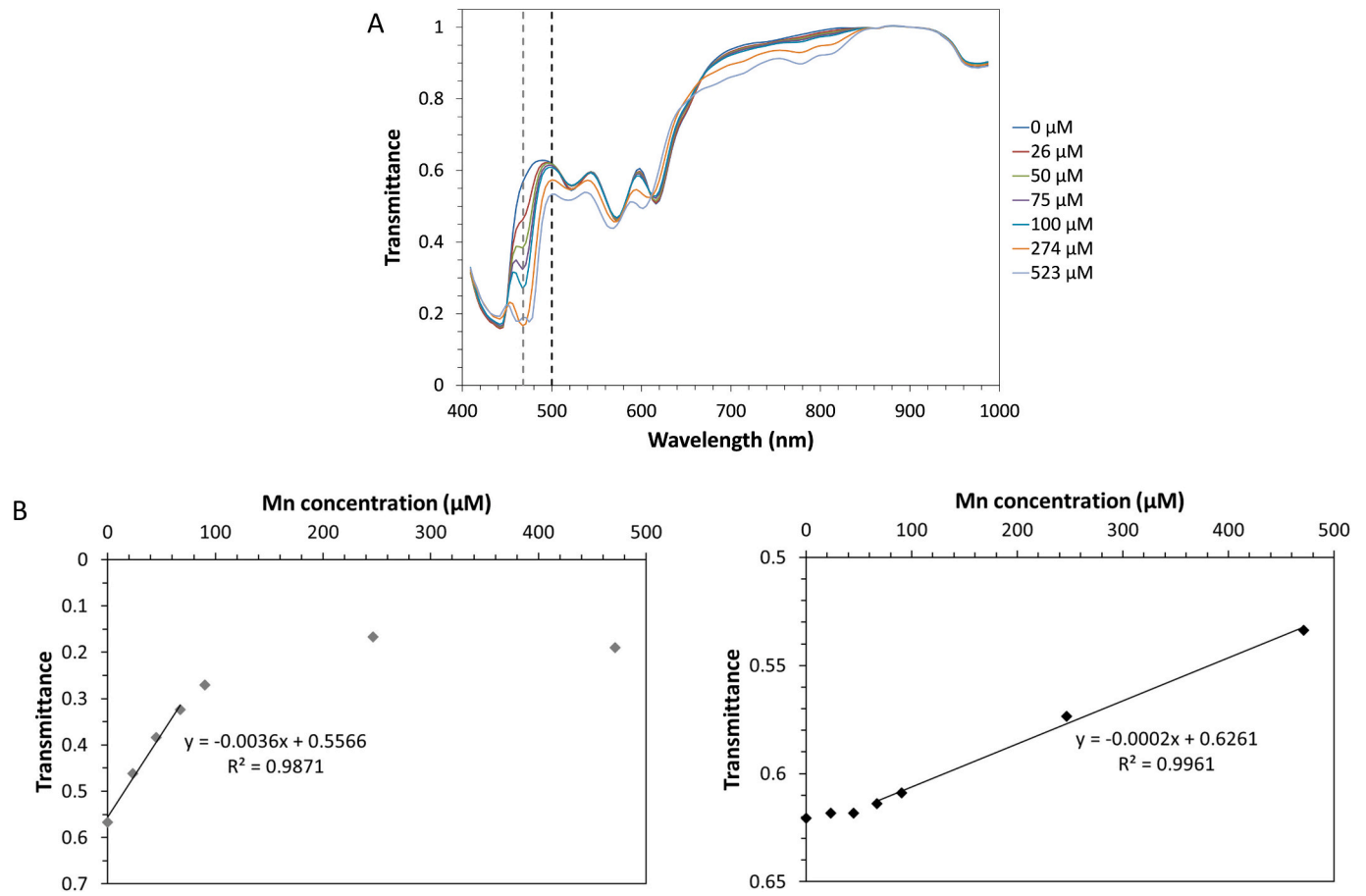

Fig. 5. A) Transmittance spectra obtained from a standard gel using a hyperspectral camera. B) Calibration curves for the transmittance values: on the left, at 470 nm and on the right at 500 nm.

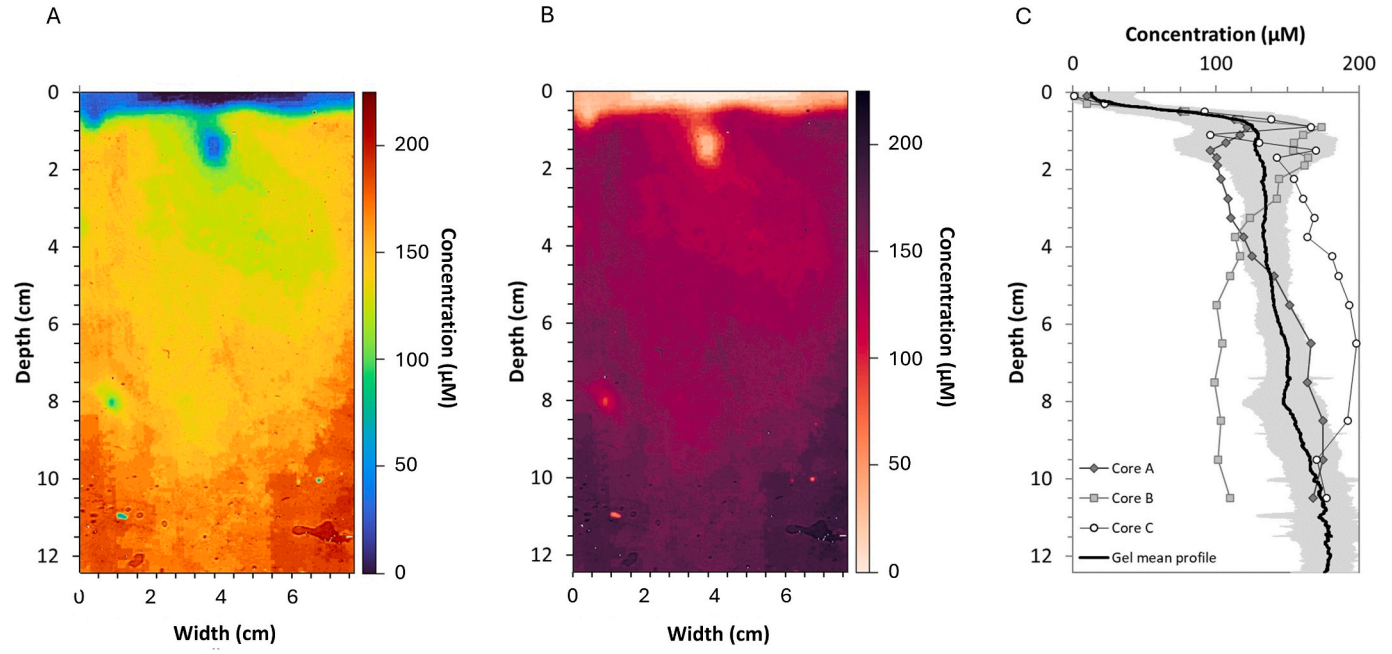

Fig. 6. *In situ* measurement of 2D manganese concentration distribution in the Bourgneuf Bay at low tide; A) image with a perceptually uniform rainbow color scale (Turbo); B) image with a uniform linear scale (Rocket) to improve image readability for all readers; C) Comparison between Mn profiles obtained from sediment cores (A, B, C) with porewater extraction and the profile obtained by calculating the average concentration of each pixel line of the 2D Mn image, where the grey area indicates 2 standard deviations (to represent 95 % of the data).

sensitivity and can be used to extend the measuring range with a linear relationship within 75–520 μM (Fig. 5).

3.6. Validation with coastal sediments

A 2D-DET probe was deployed at low tide in Bourgneuf Bay and compared with porewater profiling obtained from sliced and centrifuged sediment cores (Fig. 6). The 2D distribution of manganese after calibration of the images obtained with a flatbed scanner shows that concentrations increase rapidly below the interface to values between 84 and 172 μM at 1 cm depth. Deeper, Mn concentrations increase more slowly, reaching values between 160 and 200 μM at 12 cm depth. The average profile calculated using the 2D-DET probe (mean concentration of each pixel line) shows a profile of the same order of magnitude as the Mn profiles obtained using ICP-OES porewaters analysis. The strong increase in Mn concentration below the air-sediment interface is consistent with rapid oxygen depletion at depth (oxygen penetration depth was measured to be 1.8 ± 0.2 mm from 14 profiles realized in the dark with Unisense Clark-type electrodes, data not shown). Below the sharp concentrations at the surface, a 1 cm wide ovoid depletion is observed from the sediment surface down to 2 cm depth (Fig. 6 A and B). The lowest concentration in this feature is ~30 μmol L^{-1} while the surrounding concentrations are ~125 μmol L^{-1}. This depletion can be interpreted as a potential macrofaunal burrow. Several burrow-dwelling species were observed at the La Coupelasse site in Bourgneuf Bay (*Macoma balthica, Hediste diversicolor, Scrobicularia plana, Retusa obtusa, Nephtys hombergii* (Drouet et al., 2015)). When burrow-dwelling animals ventilate, they renew the water of their burrow with oxygen-rich and Mn-poor overlying water during immersion. Burrow lumens are thus strongly depleted in dissolved Mn compared to the surrounding sediment, allowing a diffusive flux of dissolved Mn into the lumens of the burrows. The rapid water exchange between the sediment and the overlying water represents a bioirrigational flux of dissolved Mn from sediment towards overlying water. Thibault de Chanvalon et al. (2017) developed a mathematical approach to quantify iron production rates and fluxes from Fe 2D-DET gels, and to estimate the diffusive flux across the sediment-water interface and the bioirrigational flux using identified burrow features. They showed that bioirrigation can account for 80 % of iron efflux in a mudflat in the Loire estuary. This approach could be adapted to calculate dissolved Mn fluxes using Mn 2D-DET. The presence of burrows and the relative heterogeneity of this type of environment are also likely to explain the differences between profiles and the encompassing of the average concentration profile and standard deviation of the gel by triplicate core profiles (Fig. 6C).

In the laboratory experiment conducted in an aquarium with homogenized sediment and aerated overlying seawater where specimens of polychaetes were inserted (*Hediste diversicolor*), Mn 2D features are different, even though the general vertical trend is about the same as for the *in situ* experiment in Bourgneuf Bay. A rapid increase of dissolved Mn was observed within the first 2 cm below the water-sediment interface, followed by a stabilization of concentrations at around 80 μM (Fig. 7). Differences with the previous experiment lie in the higher lateral heterogeneity, especially at the sediment-water interface, and in the fact that the 2D feature attributed to bioirrigation *in situ* generates Mn depletion (Fig. 6), while here the biogenic feature seems to enrich the environment. Indeed, an increase in dissolved manganese can be observed almost every 2 cm laterally, close to the sediment water interface (arrows B, C and D) or above (arrow A). The composition of overlying water is not homogeneous despite the agitation induced by bubbling. The 2D image for dissolved iron shows almost exactly the same 2D features. These zones coincided with the position of *Hediste diversicolor* burrows. In a previous study conducted *in situ* in an estuarine mudflat, polychaete burrows generated both depleted and enriched environments for iron and phosphorus (Thibault de Chanvalon et al., 2015, 2017). Oxygen imaging using a planar optode showed previously in another study that burrow flushing can result in plumes of anoxic water being expelled from the sediment (Volkenborn et al., 2012). Associated with this anoxic water, dissolved Mn and Fe could be transferred into the overlying water before their oxidation, as suggested by the present study. The plumes are particularly visible in the overlying water of the Fe gel image. As Fe oxidation is faster than Mn oxidation (Martin, 2005; Wang and Van Cappellen, 1996), this could lead to oxidation of dissolved iron within the aerated gel, resulting in an accumulation of iron oxide nanoparticles within the gel. As ascorbic acid is used in the Fe reagent, it could reduce these putative nano-oxides, allowing a reaction with ferrozine.

Finally, the Fe and Mn gels managed to highlight heterogeneities in the sedimentary environment. In addition to the features below the interface related to burrow outlets, both images showed the same Mn and Fe depleted zone between 3 and 5 cm depth, which could result from effective burrow ventilation. The image is sharper for Fe than for Mn. One explanation could be that Fe concentrations are generally higher than Mn concentrations in coastal sediments, generating stronger gradients. The sharper Fe image could also be due to the different oxidation kinetics of Fe and Mn. As dissolved Fe is oxidized more rapidly, sharper features are visible where Fe(II) is oxidized to Fe(III). Conversely, the slower kinetics of Mn(II) oxidation would result in greater diffusion of Mn across oxic-anoxic boundaries in the sediment and therefore a more blurred image. Finally, another analytical explanation is that the colorimetric reaction of manganese (35 min) is slower than that of iron (5 min), resulting in smoother chemical gradients for Mn due to a longer relaxation time.

4. Conclusion

The results obtained in this study clearly demonstrate the capability of this new method combining DET and colorimetry to map dissolved manganese at millimeter scale. Using a hyperspectral camera instead of a flatbed scanner increases the measuring range from 300 μM to 520 μM and lowers the detection limit from 15 μM to 5 μM. However, flatbed scanner remains a cheap and suitable tool for working in a wide range of environments. Burrow structures can be identified in both Mn and combined Fe images, highlighting the role of bioirrigation in benthic Mn fluxes. Using Mn images, the mathematical approach previously used to quantify Fe bioirrigational fluxes could be adapted to quantify Mn bioirrigational fluxes.

This new technique is easy and fast to use and provides the potential to explore the reactivity of sedimentary microenvironments towards Mn in two dimensions in a wide range of laboratory and *in situ* studies.

Funding

This work was funded by the French National Program MANGA-2D (CNRS-INSU) and by the MUDSURV project (OSUNA).

CRediT authorship contribution statement

Aurélia Mouret: Writing – original draft, Visualization, Validation, Supervision, Project administration, Methodology, Investigation, Funding acquisition, Formal analysis, Data curation, Conceptualization. **Constance Choquel:** Writing – review & editing, Visualization, Data curation. **Aubin Thibault de Chanvalon:** Writing – review & editing, Visualization, Methodology, Investigation. **Florian Cesbron:** Writing – review & editing, Methodology. **Thierry Jauffrais:** Writing – review & editing, Formal analysis. **Didier Jézéquel:** Writing – review & editing, Methodology, Conceptualization. **Patrick Launeau:** Methodology, Data curation. **Anthony Barbe:** Visualization, Validation, Methodology, Formal analysis, Data curation. **Romain Levrard:** Methodology, Formal analysis, Data curation. **Alan Nicol:** Methodology, Formal analysis, Data curation. **Céline Charbonnier:** Writing – review & editing, Methodology. **Edouard Metzger:** Writing – original draft, Validation, Supervision, Project administration, Methodology, Investigation,

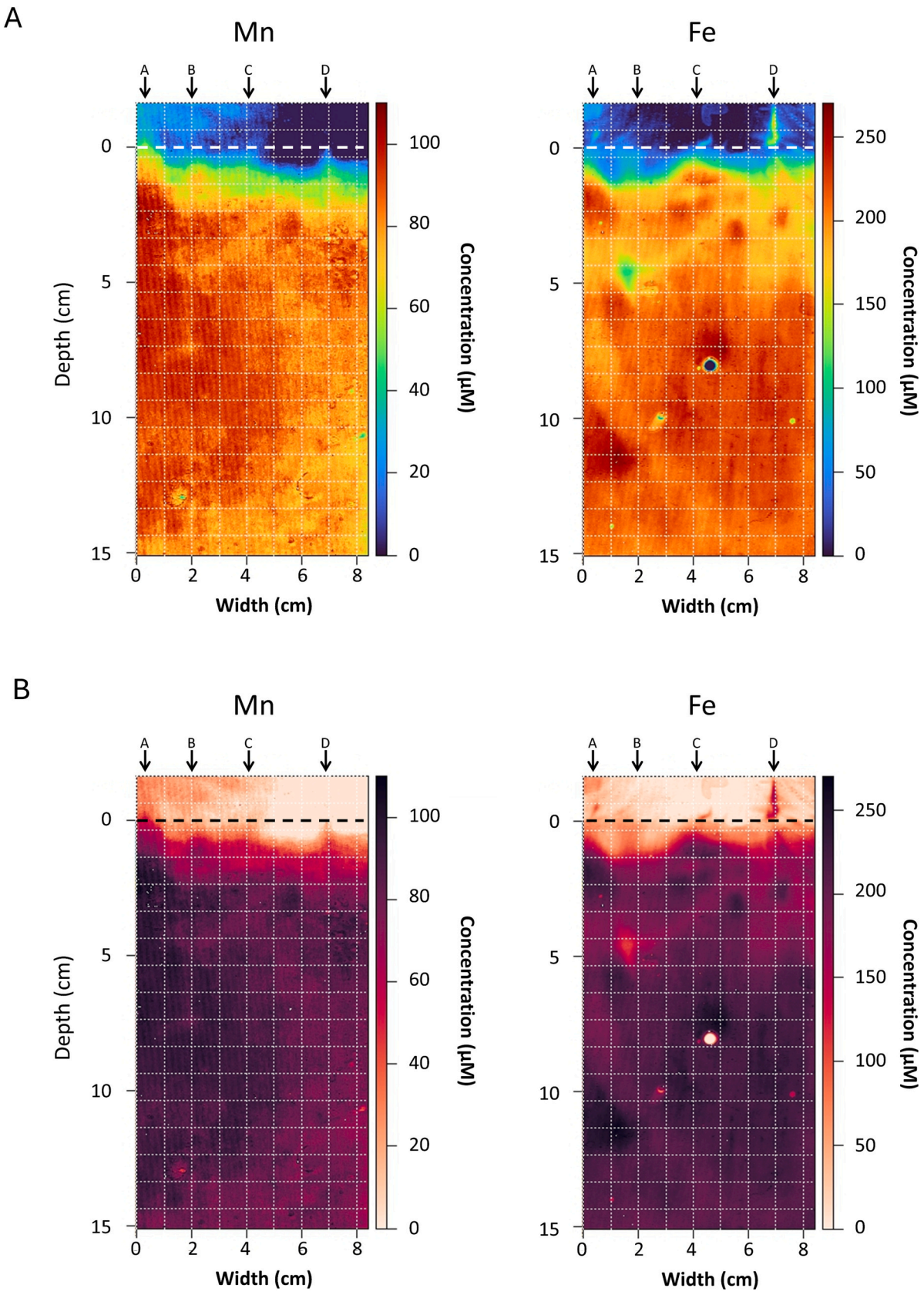

Fig. 7. 2D distributions of dissolved manganese and iron concentrations in sieved and homogenized sediments bioturbated by polychaetes and overlain by natural seawater. Mn and Fe images are stackable. A, B, C and arrows indicate the positions of polychaete burrows. A) Mn and Fe images with a perceptually uniform rainbow color scale (Turbo). The SWI is represented by a white dashed line at 0 cm depth; B) Mn and Fe images with a uniform linear scale (Rocket) to improve image readability for all readers. The SWI is represented by a black dashed line at 0 cm depth.

Funding acquisition, Conceptualization.

Data availability

Data will be made available on request.

Acknowledgment

The authors gratefully acknowledge Eric Bénéteau, who helped with the sampling for the Bourgneuf Bay survey and with ICP-AES analyses, Carole La, who helped with ICP-AES analyses, and Manuel Giraud, who helped with hyperspectral acquisitions. We also thank Charlotte LeKieffre for the discussions on the "0.4/0.8 gels dilemma".

References

Aller, R.C., Charnock, H., Edmond, J.M., McCave, I.N., Rice, A.L., Wilson, T.R.S., 1990. Bioturbation and manganese cycling in hemipelagic sediments. Philosoph. Transact. Roy. Soc. Lond. Ser. A, Math. Phys. Sci. 331, 51–68. https://doi.org/10.1098/rsta.1990.0056.

Anschutz, P., Dedieu, K., Desmazes, F., Chaillou, G., 2005. Speciation, oxidation state, and reactivity of particulate manganese in marine sediments. Chem. Geol. 218, 265–279. https://doi.org/10.1016/j.chemgeo.2005.01.008.

Bennett, W.W., Welsh, D.T., Serriere, A., Panther, J.G., Teasdale, P.R., 2015. A colorimetric DET technique for the high-resolution measurement of two-dimensional alkalinity distributions in sediment porewaters. Chemosphere 119, 547–552. https://doi.org/10.1016/j.chemosphere.2014.07.042.

Brendel, P.J., Luther, G.W.I., 1995. Development of a gold amalgam voltammetric microelectrode for the determination of dissolved Fe, Mn, O2, and S (-II) in porewaters of marine and freshwater sediments. Environ. Sci. Technol. 29, 751–761.

Burdige, D.J., 1993. The biogeochemistry of manganese and iron reduction in marine sediments. Earth Sci. Rev. 35, 249–284. https://doi.org/10.1016/0012-8252(93)90040-E.

Burle, E., Kirby-Smith, W.W., 1979. Application of formaldoxime colorimetric method for the determination of manganese in the pore water of anoxic estuarine sediments. Estuaries 2, 198–201. https://doi.org/10.2307/1351736.

Canfield, D.E., Jørgensen, B.B., Fossing, H., Glud, R., Gundersen, J., Ramsing, N.B., Thamdrup, B., Hansen, J.W., Nielsen, L.P., Hall, P.O.J., 1993a. Pathways of organic carbon oxidation in three continental margin sediments. Marine Geol. Marine Sed. Burial, Pore Water Chem. Microbiol. Diagen. 113, 27–40. https://doi.org/10.1016/0025-3227(93)90147-N.

Canfield, D.E., Thamdrup, B., Hansen, J.W., 1993b. The anaerobic degradation of organic matter in Danish coastal sediments: Iron reduction, manganese reduction, and sulfate reduction. Geochim. Cosmochim. Acta 57, 3867–3883. https://doi.org/10.1016/0016-7037(93)90340-3.

Castillejos Sepúlveda, A., Metzger, E., Littmann, S., Taubner, H., Chennu, A., Gatti, L., de Beer, D., Klatt, J.M., 2023. Two-dimensional mapping of arsenic concentration and speciation with diffusive equilibrium in thin-film gels. Environ. Sci. Technol. 57, 8107–8117. https://doi.org/10.1021/acs.est.3c00887.

Cesbron, F., Metzger, E., Launeau, P., Deflandre, B., Delgard, M.-L., Thibault de Chanvalon, A., Geslin, E., Anschutz, P., Jézéquel, D., 2014. Simultaneous 2D Imaging of Dissolved Iron and Reactive Phosphorus in Sediment Porewaters by Thin-Film and Hyperspectral Methods. Environmental Science & Technology, pp. 2816–2826.

Charbonnier, C., Anschutz, P., 2019. Spectrophotometric determination of manganese in acidified matrices from (pore)waters and from sequential leaching of sediments. Talanta 195, 778–784. https://doi.org/10.1016/j.talanta.2018.12.012.

Chiswell, B., Rauchle, G., Pascoe, M., 1990. Spectrophotometric methods for the determination of manganese. Talanta 37, 237–259. https://doi.org/10.1016/0039-9140(90)80029-F.

Davison, W., Zhang, H., 1994. In situ speciation measurements of trace components in natural waters using thin-film gels. Nature 367, 546–548. https://doi.org/10.1038/367546a0.

Davison, William, Zhang, Hao, Grime, G.W., 1994. Performance characteristics of gel probes used for measuring the chemistry of pore waters. Environ. Sci. Technol. 28, 1623–1632. https://doi.org/10.1021/es00058a015.

Dočekalová, H., Clarisse, O., Salomon, S., Wartel, M., 2002. Use of constrained DET probe for a high-resolution determination of metals and anions distribution in the sediment pore water. Talanta 57, 145–155. https://doi.org/10.1016/S0039-9140(01)00679-8.

Drouet, S., Turpin, V., Godet, L., Cognie, B., Cosson, R.P., Decottignies, P., 2015. Utilisation of intertidal mudflats by the dunlin *Calidris alpina* in relation to microphytobenthic biofilms. J. Ornithol. 156, 75–83. https://doi.org/10.1007/s10336-014-1133-x.

Echappé, C., Gernez, P., Méléder, V., Jesus, B., Cognie, B., Decottignies, P., Sabbe, K., Barillé, L., 2018. Satellite remote sensing reveals a positive impact of living oyster reefs on microalgal biofilm development. Biogeosciences 15, 905–918. https://doi.org/10.5194/bg-15-905-2018.

Froelich, P.N., Klinkhammer, G.P., Bender, M.L., Luedtke, N.A., Heath, G.R., Cullen, D., Dauphin, P., Hammond, D., Hartman, B., Maynard, V., 1979. Early oxidation of organic matter in pelagic sediments of the eastern equatorial Atlantic: suboxic diagenesis. Geochim. Cosmochim. Acta 43, 1075–1090. https://doi.org/10.1016/0016-7037(79)90095-4.

Gobeil, C., Macdonald, R.W., Sundby, B., 1997. Diagenetic separation of cadmium and manganese in suboxic continental margin sediments. Geochim. Cosmochim. Acta 61, 4647–4654. https://doi.org/10.1016/S0016-7037(97)00255-X.

Harper, M.P., Davison, W., Tych, W., 1997. Temporal, spatial, and resolution constraints for in situ sampling devices using diffusional equilibration: Dialysis and DET. Environ. Sci. Technol. 31, 3110–3119.

Ishii, H., Koh, H., Satoh, K., 1982. Spectrophotometric determination of manganese utilizing metal ion substitution in the cadmium-α,β,-γ,δ -tetrakis(4-carboxyphenyl) porphine complex. Anal. Chim. Acta 136, 347–352. https://doi.org/10.1016/S0003-2670(01)95395-4.

Jézéquel, D., Brayner, R., Metzger, E., Viollier, E., Prévot, F., Fiévet, F., 2007. Two-dimensional determination of dissolved iron and sulfur species in marine sediment pore-waters by thin-film based imaging. Thau lagoon (France). Estuar. Coast. Shelf Sci. Biogeochem. Contamin. Cycl. Sediments Human-Impact. Coast. Lagoon 72, 420–431. https://doi.org/10.1016/j.ecss.2006.11.031.

Kankanamge, N.R., Bennett, W.W., Teasdale, P.R., Huang, J., Welsh, D.T., 2020. A new colorimetric DET technique for determining mm-resolution sulfide porewater distributions and allowing improved interpretation of iron(II) co-distributions. Chemosphere 244, 125388. https://doi.org/10.1016/j.chemosphere.2019.125388.

Launeau, P., Méléder, V., Verpoorter, C., Barillé, L., Kazemipour-Ricci, F., Giraud, M., Jesus, B., Le Menn, E., 2018. Microphytobenthos biomass and diversity mapping at different spatial scales with a hyperspectral optical model. Remote Sens. 10, 716. https://doi.org/10.3390/rs10050716.

Le Houedec, S., Thibault de Chanvalon, A., Mouret, A., Metzger, E., Launeau, P., Gaudin, P., Lebeau, T., 2019. 2D image quantification of microbial iron chelators (Siderophores) using diffusive equilibrium in thin films method. Anal. Chem. 91, 1399–1407. https://doi.org/10.1021/acs.analchem.8b04021.

Lewis, B.L., Landing, W.M., 1991. The biogeochemistry of manganese and iron in the Black Sea. Deep Sea Res. Part A. Oceanogr. Res. Papers, Black Sea Oceanogr.: Results 1988 Black Sea Exped. 38, S773–S803. https://doi.org/10.1016/S0198-0149(10)80009-3.

Luther, G.W., Sundby, B., Lewis, B.L., Brendel, P.J., Silverberg, N., 1997. Interactions of manganese with the nitrogen cycle: alternative pathways to dinitrogen. Geochim. Cosmochim. Acta 61, 4043–4052. https://doi.org/10.1016/S0016-7037(97)00239-1.

Luther, G.W.I., 2010. The Role of One- and Two-Electron Transfer Reactions in Forming Thermodynamically Unstable Intermediates as Barriers in Multi-Electron Redox Reactions.

Madison, A.S., Tebo, B.M., Luther, G.W., 2011. Simultaneous determination of soluble manganese(III), manganese(II) and total manganese in natural (pore)waters. Talanta 84, 374–381. https://doi.org/10.1016/j.talanta.2011.01.025.

Madison, A.S., Tebo, B.M., Mucci, A., Sundby, B., Luther, G.W., 2013. Abundant porewater Mn(III) is a major component of the sedimentary redox system. Science 341, 875–878. https://doi.org/10.1126/science.1241396.

Martin, S., 2005. Precipitation and dissolution of Iron and manganese oxides. Environ. Catal. https://doi.org/10.1201/9781420027679.ch3.

Metzger, E., Thibault de Chanvalon, A., Cesbron, F., Barbe, A., Launeau, P., Jézéquel, D., Mouret, A., 2016. Simultaneous Nitrite/Nitrate imagery at Millimeter scale through the Water–Sediment interface. Environ. Sci. Technol. 50, 8188–8195. https://doi.org/10.1021/acs.est.6b00187.

Metzger, E., Barbe, A., Cesbron, F., Thibault de Chanvalon, A., Jauffrais, T., Jézéquel, D., Mouret, A., 2019. Two-dimensional ammonium distribution in sediment pore waters using a new colorimetric diffusive equilibration in thin-film technique. Water Res. X 2, 100023. https://doi.org/10.1016/j.wroa.2018.100023.

Murray, J.W., Dillard, J.G., Giovanoli, R., Moers, H., Stumm, W., 1985. Oxidation of Mn (II): initial mineralogy, oxidation state and ageing. Geochim. Cosmochim. Acta 49, 463–470. https://doi.org/10.1016/0016-7037(85)90038-9.

Oldham, V.E., Jones, M.R., Tebo, B.M., Luther, G.W., 2017a. Oxidative and reductive processes contributing to manganese cycling at oxic-anoxic interfaces. Marine Chem., SI: Honor. Frank Millero 195, 122–128. https://doi.org/10.1016/j.marchem.2017.06.002.

Oldham, V.E., Miller, M.T., Jensen, L.T., Luther, G.W., 2017b. Revisiting Mn and Fe removal in humic rich estuaries. Geochim. Cosmochim. Acta 209, 267–283. https://doi.org/10.1016/j.gca.2017.04.001.

Oldham, V.E., Mucci, A., Tebo, B.M., Luther, G.W., 2017c. Soluble Mn(III)–L complexes are abundant in oxygenated waters and stabilized by humic ligands. Geochim. Cosmochim. Acta 199, 238–246. https://doi.org/10.1016/j.gca.2016.11.043.

Owings, S.M., Bréthous, L., Eitel, E.M., Fields, B.P., Boever, A., Beckler, J.S., Bombled, B., Lansard, B., Metzger, E., Rabouille, C., Taillefert, M., 2021. Differential manganese and iron recycling and transport in continental margin sediments of the northern Gulf of Mexico. Mar. Chem. 229, 103908 https://doi.org/10.1016/j.marchem.2020.103908.

Pagès, A., Teasdale, P.R., Robertson, D., Bennett, W.W., Schäfer, J., Welsh, D.T., 2011. Representative measurement of two-dimensional reactive phosphate distributions and co-distributed iron(II) and sulfide in seagrass sediment porewaters. Chemosphere 85, 1256–1261. https://doi.org/10.1016/j.chemosphere.2011.07.020.

Robertson, D., Teasdale, P.R., Welsh, D.T., 2008. A novel gel-based technique for the high resolution, two-dimensional determination of iron (II) and sulfide in sediment. Limnol. Oceanogr. Methods 6, 502–512. https://doi.org/10.4319/lom.2008.6.502.

Schneider, C.A., Rasband, W.S., Eliceiri, K.W., 2012. NIH image to ImageJ: 25 years of image analysis. Nat. Methods 9, 671–675. https://doi.org/10.1038/nmeth.2089.

Shuttleworth, Sarah M., Davison, W., Hamilton-Taylor, J., 1999. Two-dimensional and fine structure in the concentrations of Iron and manganese in sediment pore-waters. Environ. Sci. Technol. 33, 4169–4175. https://doi.org/10.1021/es990184l.

Soto-Neira, J., Zhu, Q., Aller, R.C., 2011a. A new spectrophotometric method to quantify dissolved manganese in marine pore waters. Mar. Chem. 127, 56–63. https://doi.org/10.1016/j.marchem.2011.07.009.

Soto-Neira, J., Zhu, Q., Aller, R.C., 2011b. A new spectrophotometric method to quantify dissolved manganese in marine pore waters. Mar. Chem. 127, 56–63. https://doi.org/10.1016/j.marchem.2011.07.009.

Sundby, B., Silverberg, N., 1985. Manganese fluxes in the benthic boundary layer1. Limnol. Oceanogr. 30, 372–381. https://doi.org/10.4319/lo.1985.30.2.0372.

Swinbanks, D.D., Shirayama, Y., 1984. Burrow stratigraphy in relation to manganese diagenesis in modern deep-sea carbonates. Deep Sea Res. Part A. Oceanogr. Res. Papers 31, 1197–1223. https://doi.org/10.1016/0198-0149(84)90058-X.

Tebo, B.M., 1991. Manganese(II) oxidation in the suboxic zone of the Black Sea. Deep Sea Res. Part A. Oceanogr. Res. Papers, Black Sea Oceanogr.: Results 1988 Black Sea Exped. 38, S883–S905. https://doi.org/10.1016/S0198-0149(10)80015-9.

Thamdrup, B., Fossing, H., Jørgensen, B.B., 1994. Manganese, iron and sulfur cycling in a coastal marine sediment, Aarhus bay, Denmark. Geochim. Cosmochim. Acta 58, 5115–5129. https://doi.org/10.1016/0016-7037(94)90298-4.

Thibault de Chanvalon, A., Luther, G.W., 2019. Mn speciation at nanomolar concentrations with a porphyrin competitive ligand and UV–vis measurements. Talanta 200, 15–21. https://doi.org/10.1016/j.talanta.2019.02.069.

Thibault de Chanvalon, A., Metzger, E., Mouret, A., Cesbron, F., Knoery, J., Rozuel, E., Launeau, P., Nardelli, M.P., Jorissen, F.J., Geslin, E., 2015. Two-dimensional distribution of living benthic foraminifera in anoxic sediment layers of an estuarine mudflat (Loire estuary, France). Biogeosciences 12, 6219–6234. https://doi.org/10.5194/bg-12-6219-2015.

Thibault de Chanvalon, A., Metzger, E., Mouret, A., Knoery, J., Geslin, E., Meysman, F.J. R., 2017. Two dimensional mapping of iron release in marine sediments at submillimetre scale. Mar. Chem. 191, 34–49. https://doi.org/10.1016/j.marchem.2016.04.003.

Trouwborst, R.E., Clement, B.G., Tebo, B.M., Glazer, B.T., Luther, G.W., 2006. Soluble Mn(III) in Suboxic zones. Science 313, 1955–1957. https://doi.org/10.1126/science.1132876.

Volkenborn, N., Meile, C., Polerecky, L., Pilditch, C.A., Norkko, A., Norkko, J., Hewitt, J. E., Thrush, S.F., Wethey, D.S., Woodin, S.A., 2012. Intermittent bioirrigation and oxygen dynamics in permeable sediments: an experimental and modeling study of three tellinid bivalves. J. Mar. Res. 70, 794–823. https://doi.org/10.1357/002224012806770955.

Wang, Y., Van Cappellen, P., 1996. A multicomponent reactive transport model of early diagenesis: application to redox cycling in coastal marine sediments. Geochim. Cosmochim. Acta 60, 2993–3014.

Zhang, H., Davison, W., Miller, S., Tych, W., 1995. In situ high resolution measurements of fluxes of Ni, Cu, Fe, and Mn and concentrations of Zn and cd in porewaters by DGT. Geochim. Cosmochim. Acta 59, 4181–4192. https://doi.org/10.1016/0016-7037(95)00293-9.